Ann. Geophys., 43, 37–54, 2025
https://doi.org/10.5194/angeo-43-37-2025

Annales Geophysicae Open Access EGU

Longitudinally spaced observations of a magnetic-cloud-like structure embedded in a co-rotating interaction region

Megan L. Maunder[1], Claire Foullon[1], Robert Forsyth[2], David Barnes[3], and Jackie A. Davies[3]

[1]Department of Mathematics and Statistics, University of Exeter, Exeter, EX4 4QF, UK
[2]Department of Physics, Imperial College London, London, SW7 2AZ, UK
[3]STFC RAL Space, Rutherford Appleton Laboratory, Harwell Campus, Oxfordshire, OX11 0QX, UK

Correspondence: Claire Foullon (c.foullon@exeter.ac.uk)

Received: 21 December 2023 – Discussion started: 10 January 2024
Revised: 22 October 2024 – Accepted: 5 November 2024 – Published: 7 January 2025

Abstract. Interaction mechanisms in the solar wind affect the evolution of magnetic structures, thereby mediating the properties acquired during their formation processes at the Sun as they propagate outward. Using remote-sensing and in situ observations across multiple spacecraft we investigate a magnetic-cloud-like structure (MCL) detected in situ on 3–4 July 2007 near the ecliptic plane at different longitudes with OMNI, STEREO-A and STEREO-B. The MCL is entrained in a corotating interaction region (CIR) originating in the northern heliospheric sector, creating a merged interaction region (MIR). Our multi-spacecraft analysis, facilitated by the small angular separation of 17° in longitude and the solar minimum background, reveals the "ageing" of the MCL–CIR interaction. Local negative expansion speeds of the MCL indicate compression increasing further downstream. Differences in size, the formation of the sheath, the presence of forward and reverse waves, and the small-scale structuring demonstrate the progression of the interaction. This unique opportunity to observe the temporal evolution of the MCL–CIR interaction highlights the intricate nature of solar wind structures and their interactions at 1 AU.

1 Introduction

The heliosphere is formed by the continuous outflow of the solar wind (Parker, 1958), in which we observe both small- and large-scale transients. Coronal mass ejections (CMEs) and their heliospheric counterparts (interplanetary CMEs, ICMEs) are large-scale transients known to drive interplanetary shocks (Gosling et al., 1975). ICMEs with magnetic clouds (MCs) are a subset of ICMEs with distinct magnetic field characteristics: an enhanced magnetic field and smooth, large-scale rotation of the magnetic field vectors (Burlaga, 1984, 2001). Marubashi (1986) and Bothmer and Schwenn (1998) suggest that a twisted magnetic flux tube can approximate the global magnetic structure of a MC, and fitting models to the magnetic field time series may provide an estimate of its large-scale topology (Lepping et al., 1990; Bothmer and Schwenn, 1998). A MC is usually identified when a spacecraft passes near its cloud axis. Magnetic cloud-like structures (MCLs) are magnetic structures identified using the same definition as a MC, except that a traditional flux-rope model cannot be fitted (Lepping et al., 2005; Foullon et al., 2007). Wu et al. (2006) found that the occurrence rate of MCLs and joint sets (MCs and MCLs) is related to both the solar activity and the CME occurrence rate. This correlation is not observed with MCs alone. It is possible that all ICMEs contain flux ropes but that some are not recognised as MCs only because the spacecraft trajectories skim the flanks (Marubashi, 1997; Kilpua et al., 2012, 2017).

Identifying ICMEs from in situ data is a challenging and somewhat ambiguous task; there are around two dozen recognised signatures (Zurbuchen and Richardson, 2006), each with its limitations (Richardson, 2014), and longitudinal separations of a few degrees between spacecraft can still result in significantly different observations and event properties (Davies et al., 2020). Single spacecraft in situ observations enable limited analysis as they are only able to measure a single track through the ICME as it passes over the spacecraft, leading to discrepancies or incomplete knowledge of the instantaneous structure and composition of ICMEs (Rus-

sell and Mulligan, 2002; Howard, 2011; DiBraccio et al., 2015). According to Kilpua et al. (2012), "ICME-like" transients are defined as lasting more than 3 h but not meeting the maximum magnetic field criteria of $(B_{\max}) > 7$ nT and duration of more than 10 h to be classed as an ICME. ICME-like transients, which are smaller than full ICMEs, fit within the continuous size distribution of magnetic flux ropes, ranging from small-sized (0.004 AU) to intermediate-sized (0.6 AU) structures (Feng et al., 2007). The identification becomes even more challenging in the case of flux ropes in complex solar wind environments (e.g. Rouillard et al., 2009; Winslow et al., 2021). In such cases, multi-spacecraft observations become key to disentangling features to give a more accurate estimation of flux-rope properties and structure of ICMEs at different points, permitting the development of a more accurate implied 3D structure (e.g. Foullon et al., 2007; Möstl et al., 2009; Palmerio et al., 2019).

Stream interaction regions (SIRs), sometimes referred to as corotating interaction regions (CIRs), are regions in which the ambient plasma is compressed (Smith and Wolfe, 1976; Pizzo and Gosling, 1994; Richardson, 2018) as a result of fast wind or high-speed stream (HSS) emerging behind slow wind from adjacent longitudinal sources interacting as they are brought into radial alignment by solar rotation. They are common high-density structures observed in situ during solar minimum (Gazis, 1996). Since coronal holes, the source of the fast wind at the Sun, tend to be long-lived, CIRs are the subset of SIRs observed at regular intervals of approximately the solar rotation period (for instance, by a single observatory in situ). Conventionally, SIRs and CIRs are associated with the streamer belt and its embedded heliospheric current sheet (HCS), which can extend north and south of the solar equator to heliographic latitudes of about $\pm 30°$. The interaction of CIRs with transients, such as CMEs, is not uncommon (e.g. Kay et al., 2023). Complex structures arising from flux-rope interactions, including interactions with the HSS, CIR/SIR or HCS, are a type of merged interaction regions (MIRs; e.g. Burlaga, 1995). While much is known about MIR formation beyond 1 AU, recent studies have increasingly focused on MIRs within or at 1 AU, primarily examining large structures with radial extents of 2 to 4 AU (e.g. Burlaga et al., 2003; Rouillard et al., 2010b; Rodkin et al., 2018), their impacts on geomagnetic and ionospheric activity (e.g. Farrugia et al., 2011), and solar wind propagation (e.g. Shugay et al., 2018).

We focus on small-scale ICMEs or ICME-like transients, likely associated with small-scale transients at the Sun. In a study by Rouillard et al. (2008), images from the Heliospheric Imager (HI) on the Solar Terrestrial Relations Observatory (STEREO) were used to attribute CIR-associated waves to continual release of small-scale transients in the slow solar wind, which are subsequently compressed in CIRs. The formation of plasmoids, or magnetic "blob" islands, in the solar wind is a complex process influenced by several mechanisms. The seemingly quiescent slow wind consists, at least in part, of transient events from magnetic reconnection generated either at the cusps of streamers or between the coronal hole boundaries and the cusps of streamers (e.g. Wang et al., 2000). Crooker and Intriligator (1996) first reported the observation of a flux-rope transient "in the HCS", showing an ICME forming a highly distended flux-rope "occlusion". Less obvious transient signatures are generally detected as multiple field reversals and smaller coiled features, which give a layered structure appearance to the HCS (e.g. Crooker et al., 2004; Foullon et al., 2009). A multi-spacecraft study of the HCS for a 2008 event looked at the slow solar wind around the HCS as a boundary layer (Foullon et al., 2011). The study allowed the observation of evolution from east to west in heliospheric longitudes, showing evidence of the continuous releases of plasmoids and a differential rotation-driven evolution leading to asymmetry by interchange. The transient release of density blobs and flux ropes through sequential magnetic reconnection at the tip of the helmet streamer has been observed with STEREO remote sensing (Sanchez-Diaz et al., 2017) and with the Parker Solar Probe in situ (Lavraud et al., 2020).

In the present study we investigate complex structures of the sector boundary observed in situ on 3–4 July 2007. Using remote-sensing and in situ observations across multiple spacecraft near the ecliptic plane with complementary methods of analysis, we demonstrate the presence of a MCL embedded in a CIR, resulting in a MIR. We present: the in situ observations of ICME or ICME-like transients at STEREO-A, STEREO-B and OMNI showing evidence for a MIR (Sect. 2); further analysis of the transients focusing on how they interact with the CIR to form the MIR (Sect. 3); a multi-spacecraft combined view of dynamics and evolution, using modelling and predictions derived from remote-sensing observations and a comparative analysis of MIR observations at different longitudes (Sect. 4); followed by a summary of our findings (Sect. 5).

A contemporaneous solar event was presented in Maunder et al. (2022), where the multi-spacecraft study of a mid-latitude CME revealed by a unique orbital configuration permitted the analysis of remote-sensing observations from the twin STEREO-A and STEREO-B spacecraft and of its subsequent in situ counterpart outside the ecliptic plane, at Ulysses. Here our study focuses on near-ecliptic in situ observations.

2 Near-ecliptic observations

2.1 Spacecraft data and configuration

We include data sets from the STEREO (STEREO-A and STEREO-B, Kaiser et al., 2008) Sun Earth Connection Coronal and Heliospheric Investigation (SECCHI) HI-1 and HI-2 cameras, with respective elongation ranges of 4–24 and 18–88° in the ecliptic plane (Eyles et al., 2009), the In situ Mea-

surements of Particles And CME Transients (IMPACT; Luhmann et al., 2008) Magnetometer, the IMPACT Solar Wind Electron Analyzer (SWEA; Luhmann et al., 2008), and the Plasma and Suprathermal Ion Composition (PLASTIC) investigation (Galvin et al., 2008). We also use in situ observations from the OMNI virtual observatory, which combines multiple near-Earth (L1) data sets, including the Advanced Composition Explorer (ACE) (Stone et al., 1998) and WIND (Lepping et al., 1995); see King and Papitashvili (2005).

The spacecraft positions on 4 July 2007 are given in Table 1 in Heliographic Earth Ecliptic coordinate system (HEE) coordinates and are shown in Fig. 1 as seen from above the north pole (panel a) and in a 3D view to the east of the Sun–Earth line (panel b). On a heliospheric scale, we can consider OMNI's position as Earth (rather than the adjusted Earth bow shock nose location). The event under study was observed very early into the STEREO mission, where both spacecraft are close to Earth; STEREO-A and STEREO-B have a longitudinal separation of 10.12 and −6.46° [HEE] from Earth respectively. Given their HEE latitudes, we will refer to the STEREO-A, OMNI and STEREO-B in situ observations as "near-ecliptic".

2.2 ICME and ICME-like transients

Figures 2, 3 and 4 show the structures observed at OMNI, STEREO-A and STEREO-B respectively. Further observations from ACE are shown in Fig. 5 to complement those at OMNI (as the ACE data are not shown in the same time frame, similar observations to those in Fig. 2 are shown for context). The MCL boundaries are indicated by magenta vertical lines, and specific MCL properties are given in Table 2. A CIR is also observed across all spacecraft, and Table 2 gives the arrival time of each part of the transient and CIR combined, which we refer to as the MIR. The combined ICME-CIR structure will be discussed as an MIR in Sect. 3.

Panels (a)–(d) of Fig. 2–5 show the magnitude and normalised components of the magnetic field vector. For the twin STEREO observations, the components are presented in the Heliographic Radial Tangential Normal (RTN) system of reference (Burlaga, 1984) and normalised. In this coordinate system, $\boldsymbol{R}$ points from the Sun to the spacecraft, $\boldsymbol{T}$ is the Sun's rotation vector crossed into $\boldsymbol{R}$ (thus towards west for a spacecraft near the ecliptic plane) and $\boldsymbol{N}$ completes the right-handed system. The magnetic field components of the OMNI and ACE observations are given in the Geocentric Solar Ecliptic (GSE) system of reference. In the OMNI and ACE data, the correspondence between GSE and RTN is then $\boldsymbol{B_X} \equiv -\boldsymbol{B_R}$, $\boldsymbol{B_Y} \equiv -\boldsymbol{B_T}$, $\boldsymbol{B_Z} \equiv \boldsymbol{B_N}$ for the magnetic field components, and so we refer to the transformed components for ease of comparison. The MCL is identified by an enhanced magnetic field followed by a clear rotation in the $\boldsymbol{B_T}$ and $\boldsymbol{B_N}$ vectors in STEREO-A and STEREO-B and in the $-\boldsymbol{B_Z}$ vector in OMNI and ACE. The flux-rope leading edge (labelled "MCL") arrives first at STEREO-B at 04:00 UT on 3 July and then at OMNI at 11:00 UT and STEREO-A at 16:16 UT the same day (time t_{MCL}). The MCL, identified between time t_{MCL} and the trailing edge at time t_{CIR}, has a mean magnetic field intensity (averaged over the time range between t_{MCL} and t_{CIR}) $\langle B \rangle = 7$, 9, 7 nT in STEREO-A, OMNI and STEREO-B respectively. The structures at STEREO-A and STEREO-B meet the ICME criteria proposed by Kilpua et al. (2012); only the MCL structure at OMNI lasts less than 10 h and can therefore be classified as an ICME-like structure.

In panel (e) of Fig. 2–4, the MCL is characterised by a consistent and relatively slow proton speed (e.g. Lepping et al., 1990), with a mean solar wind speed (and standard deviation) of 337 (± 6.8), 362 (± 14.1) and 411 (± 32.9) km s^{-1} at STEREO-A, OMNI and STEREO-B respectively (again averaged over the time range between t_{MCL} and t_{CIR}). The proton temperature, in panel (f) is below the expected solar wind temperature T_{ex} (overplotted in blue, Richardson and Cane, 1995; Lopez, 1987) for STEREO-A and OMNI, indicative of a MC, but approximately matches T_{ex} for STEREO-B. Panel (g) shows a drop in proton density. Panel (h) shows the total pressure (black), magnetic pressure (purple) and proton pressure (navy); here we observe a drop in proton pressure, consistent with the passage of a MC (Gosling, 1994; Gosling et al., 1994).

The proton beta, β_{p}, in panel (i), is consistently less than 1 across the MCL (0.01–0.38, 0.04–0.27 and 0.03–0.67 in STEREO-A, OMNI and STEREO-B respectively), and we see a distinct drop in comparison with the surrounding plasma. This is a convincing signature for all three spacecraft. For STEREO-A and STEREO-B we present the suprathermal electron pitch angle (PA) distribution, in panel (j). The ACE electron pitch angle data are shown in panel (g) of Fig. 5 (OMNI does not include pitch angle data). This is predominately anti-sunward in STEREO-A and ACE with some spreading in STEREO-B.

At STEREO-A, we observe a preceding forward pressure wave (FW1) at 07:40 UT on 3 July, characterised by pressure and speed increases. This wave, 8 h 36 min before and a result of plasma build-up at the leading edge of the MCL, is not evident in the other near-ecliptic spacecraft observations. Instead, if a pressure wave is present at OMNI and STEREO-B, it coincides with the start of the MCL (this time is shown in brackets in Table 2). Similarly, the trailing edge of the MCL at STEREO-A (labelled "CIR" – see below) coincides with a second forward wave (FW2); this is less evident at the other spacecraft. At all near-ecliptic spacecraft, a CIR achieving speeds above 600 km s^{-1} runs into the back of the MCL. At STEREO-A, this interaction drives the forward wave (FW2) at the front of the CIR (compression region). At all spacecraft, a reverse wave (RW) propagates back into the fast wind behind the CIR, marking the rear of the CIR.

Thus, FW1 and FW2 are reasonably clear at STEREO-A but not obviously present in STEREO-B and OMNI data. The front sheath (FS; between "FW1" and "MCL") and the

Table 1. Spacecraft positions on 4 July 2007.

Spacecraft	Latitude (°) [HEE]	Longitude (°) [HEE]	Radial distance (AU)
STEREO-A	0.12	10.12	0.96
OMNI (Earth)	0.00	0.00	1
STEREO-B	−0.26	−6.46	1.08

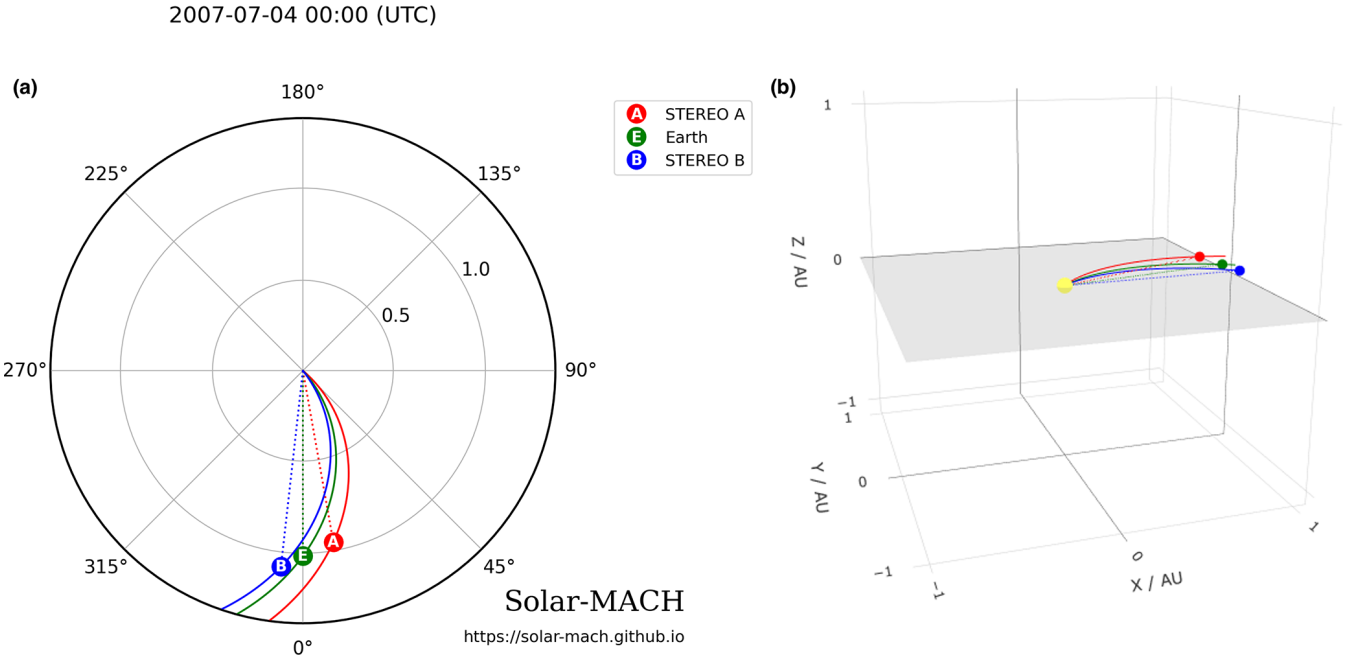

Figure 1. Spacecraft positions on 4 July 2007 obtained with the Solar MAgnetic Connection Haus (Solar-MACH) tool (Gieseler et al., 2023): **(a)** view from above the solar north pole including Earth's orbit (1 AU) and **(b)** 3D view to the east of the Sun–Earth line, showing the spacecraft above the equatorial plane (grey shading). Magnetic connections in interplanetary space are obtained by the classic Parker heliospheric magnetic field for solar wind speeds of 600 km s^{-1}.

MCL at STEREO-A form an ICME. The ICME at STEREO-B and the ICME-like transient at OMNI only contain the MCL. The MCL is followed by two distinct boundaries, "CIR/FW2" and "RW": at STEREO-A, they are the forward and reverse waves from a CIR, while at STEREO-B and OMNI, "CIR" only marks a boundary between the MCL and CIR, and "RW" marks the location of a reverse wave. Comparing the speed profile at STEREO-B with the profiles at the other spacecraft, it is possible that the wave driven by the CIR compression ("FW2") has propagated through the front of the MCL. In other words, the MCL is more entrained at STEREO-B than at the other spacecraft. The reverse wave (RW) is detected at 08:00, 08:10 and 22:00 UT on 4 July, in STEREO-B, OMNI and STEREO-A, which is 17 h 50 min, 13 h 10 min and 15 h later than the "CIR" boundary respectively.

2.3 Magnetic orientation

In Figs. 3–4, between the leading and trailing edges of the MCL, we distinguish a clear coherent rotation of the magnetic field vector with a low level of magnetic field-magnitude fluctuations and low values of proton plasma beta. Although a minimum variance analysis (MVA) did not reveal reliable axis orientations, these are clear signatures of MCLs and support the flux-rope interpretation. We adopt the method proposed by Bothmer and Schwenn (1998) and Mulligan et al. (1998) to deduce the magnetic configuration of the MCLs and the sign of helicity, the helicity being a measure that describes how the magnetic field lines are wound around each other (applied in the same manner as Dasso et al., 2006; Foullon et al., 2007; Kilpua et al., 2017). The method assumes that a MC (or MCL as in this case) possesses a specific magnetic configuration, of which the sense of the rotation indicates the sign of its helicity. We also use the suprathermal electron pitch angle characteristics from STEREO-A, STEREO-B and ACE (see Fig. 3, 4 and 5) to assist in the in-

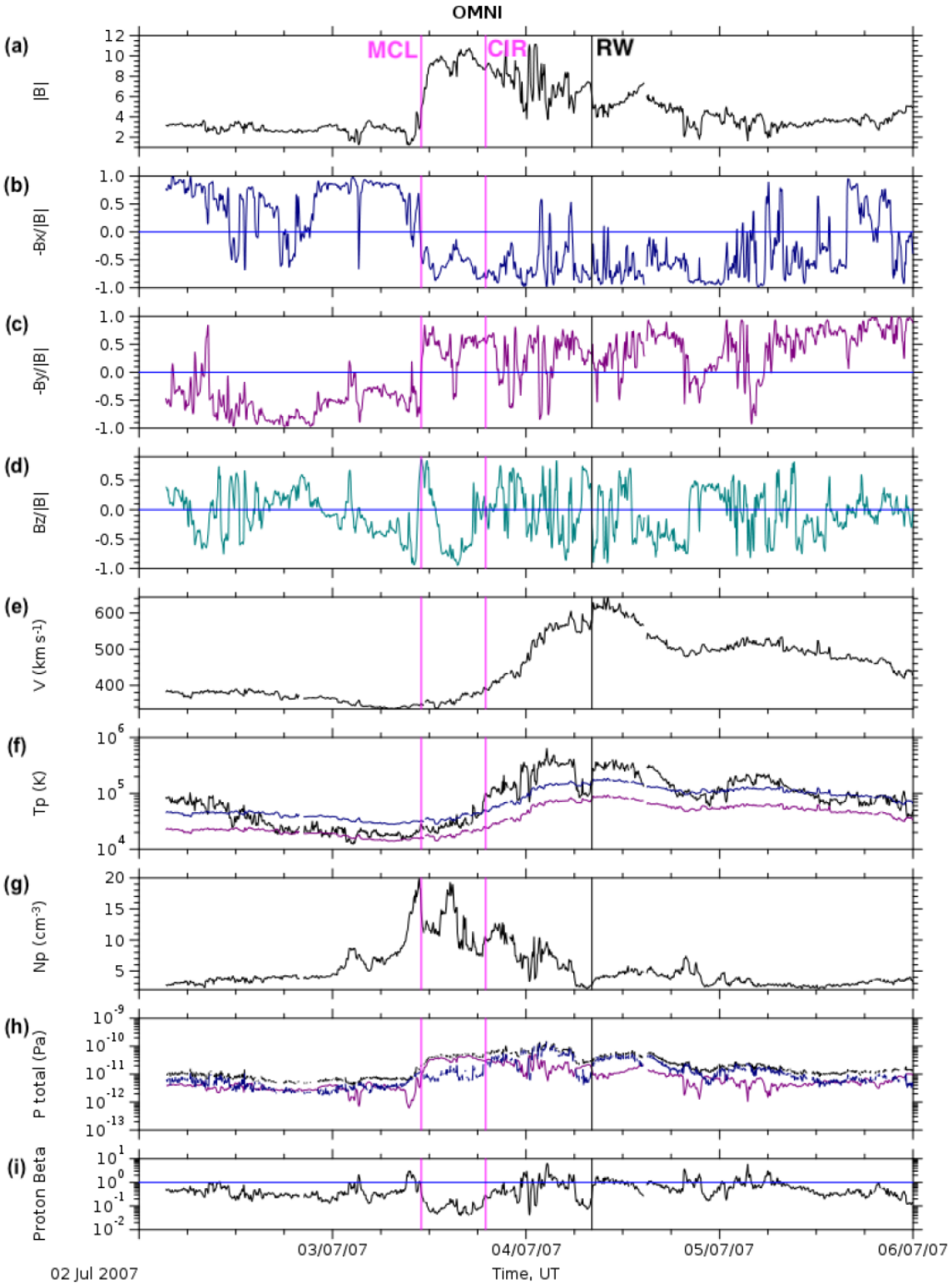

Figure 2. The MIR observed on 3–4 July 2007 by OMNI. **(a)** Magnitude and **(b–d)** normalised components of the magnetic field vector (GSE); **(e)** proton speed; **(f)** proton temperature (black), expected temperature calculated from the observed solar wind speed (blue) and half the expected proton temperature (purple); **(g)** proton density; **(h)** total pressure (black), magnetic pressure (purple) and proton pressure (navy); and **(i)** proton plasma beta with a threshold of 1 (blue). Magenta vertical lines labelled "MCL" and "CIR" represent the leading and trailing edges of the MCL respectively; the black vertical line labelled "RW" represents the reverse pressure wave behind the compression region.

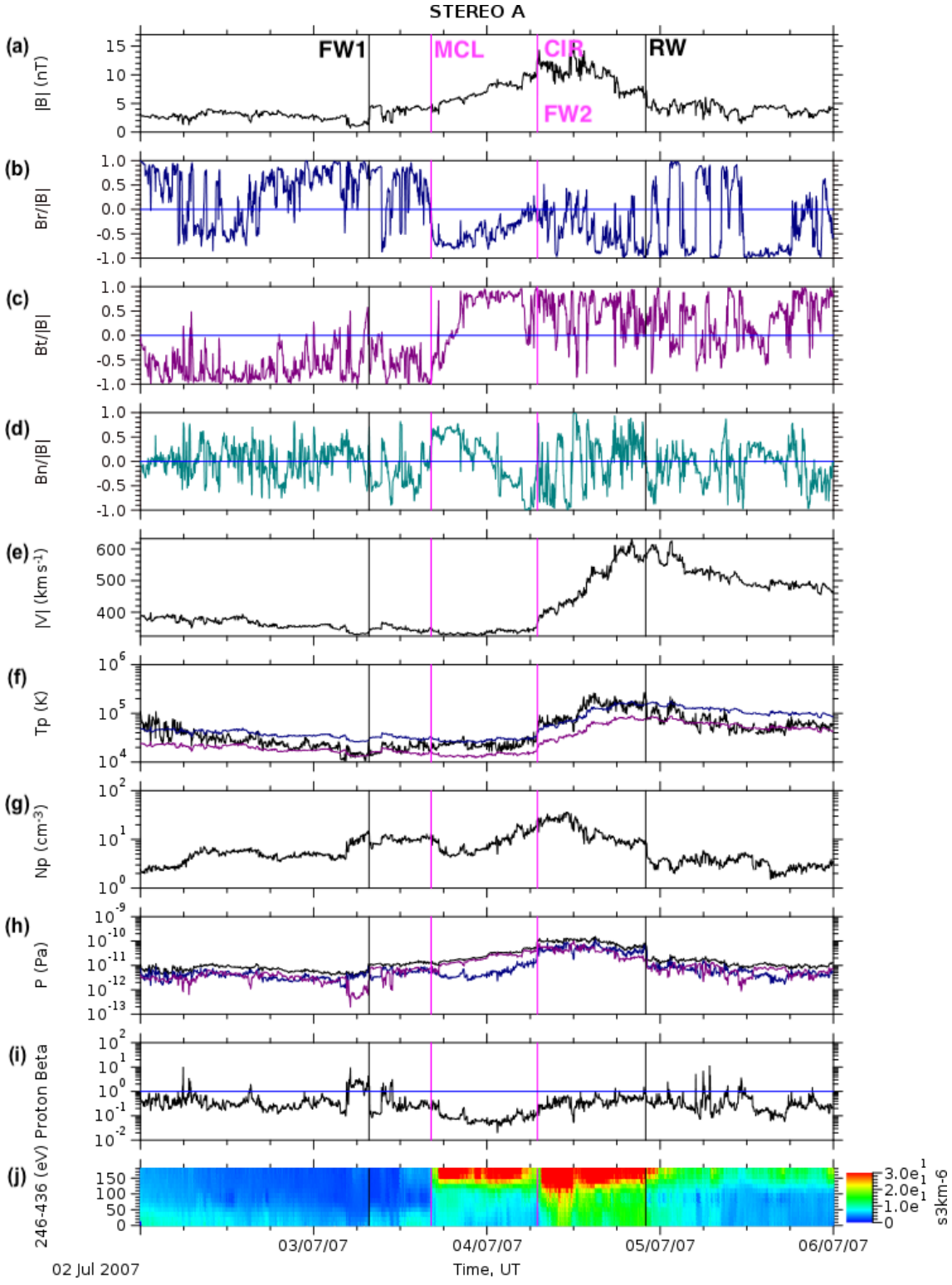

Figure 3. The MIR observed on 3 July 2007 at STEREO-A. Captions for panels and labels are as those in Fig. 2, with the magnetic field vector shown in the RTN system and the addition of **(j)** the electron pitch angles at 272 eV, the black vertical line labelled "FW1" representing the pressure wave in front of the sheath and the label "FW2" coinciding with the magenta vertical line "CIR" to represent the pressure wave created by the fast wind propagating into the back of the MCL.

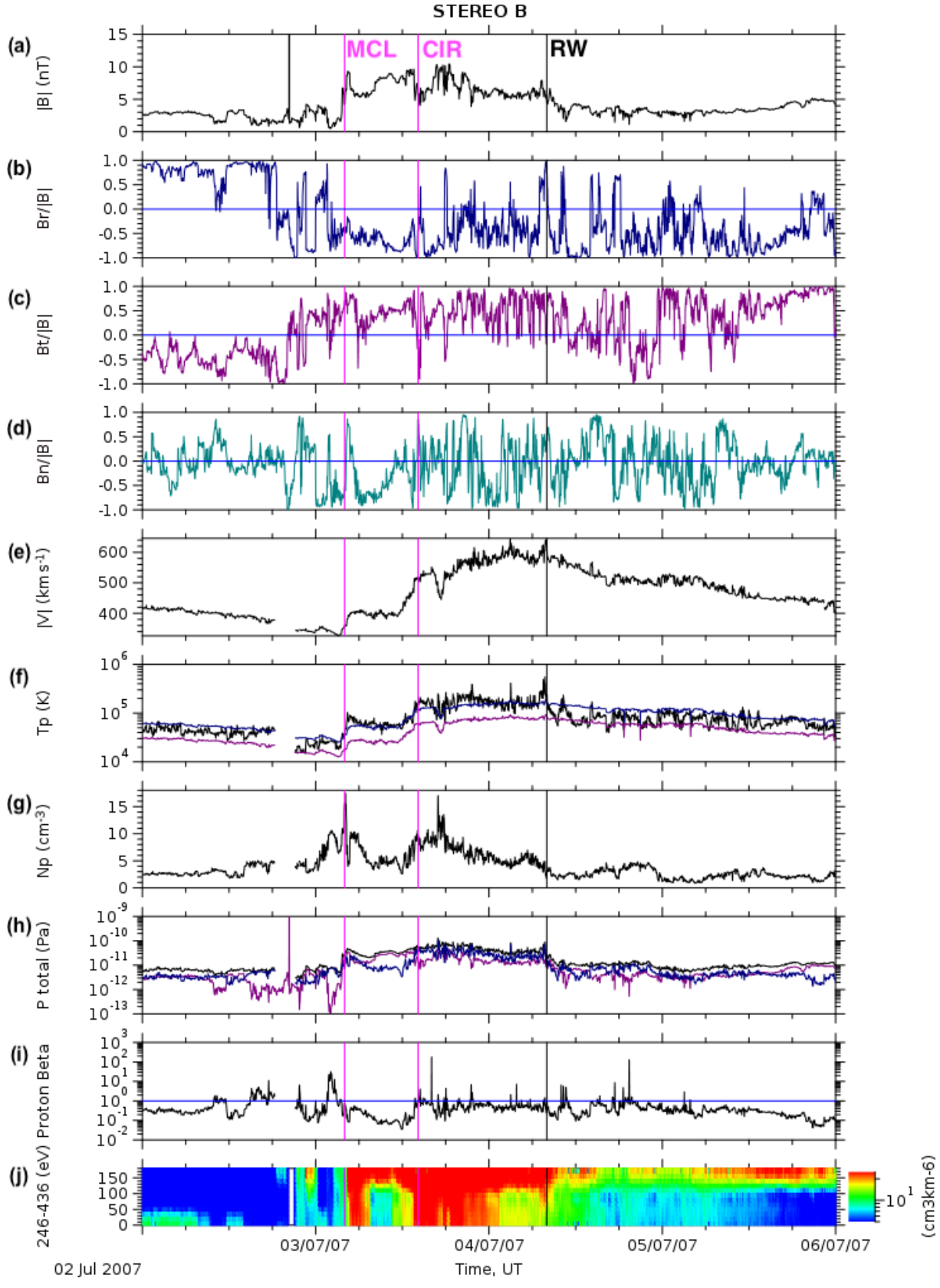

Figure 4. The MIR observed on 3–4 July 2007 by STEREO-B. Captions for panels and labels are as those in Fig. 3.

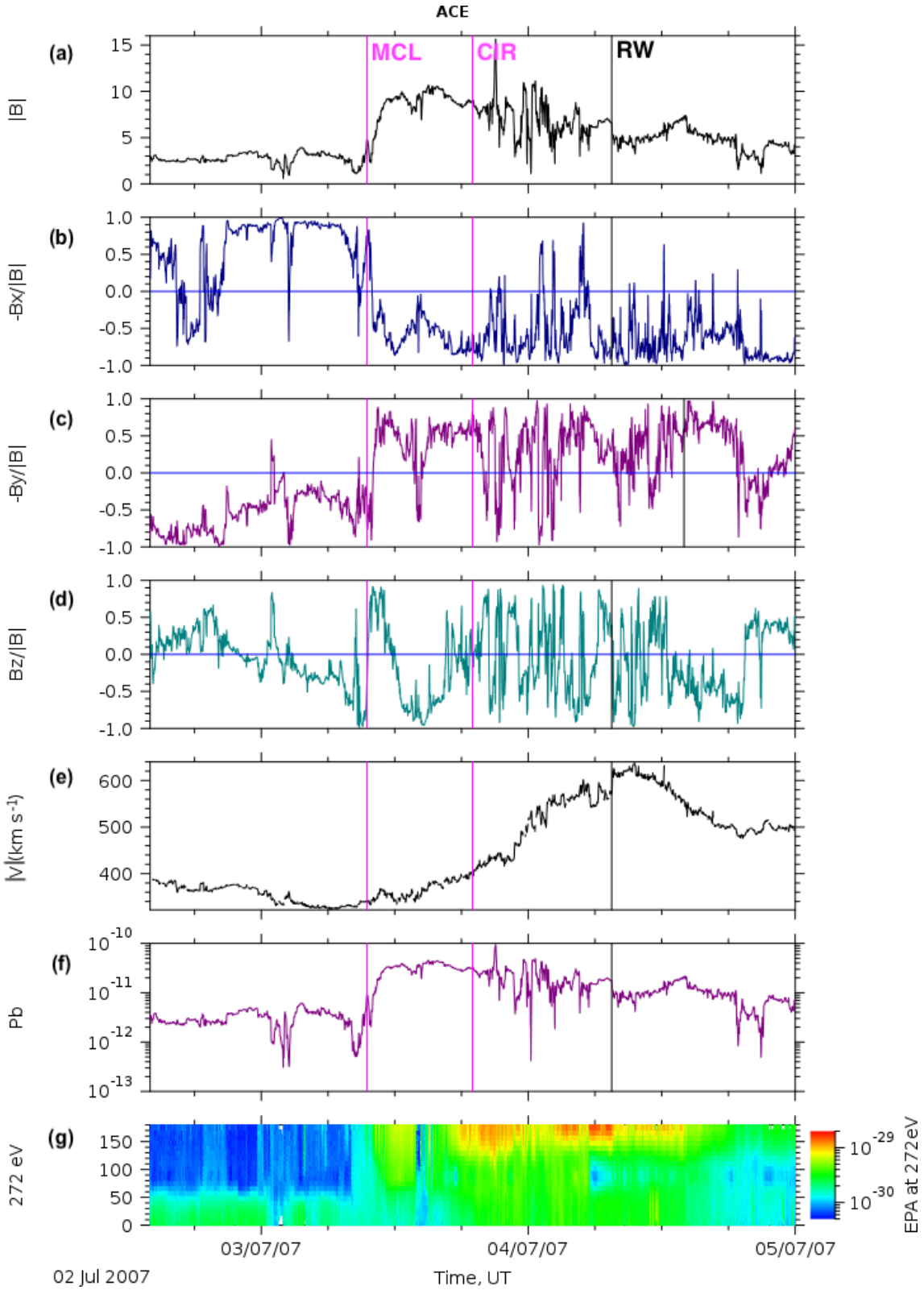

Figure 5. The MIR observed on 3–4 July 2007 by ACE. Captions for panels **(a)**–**(e)** are as in Fig. 2, **(f)** magnetic pressure (purple) as in panel **(h)** of Fig. 2 and caption for panel **(g)** as in panel **(j)** of Fig. 3.

Table 2. MIR and MCL (STEREO/OMNI) properties: the arrival time of the wave front t_{FW1}, flux-rope leading edge t_{MCL}, CIR leading edge t_{CIR}, trailing reverse waves t_{RW}, the average velocity $\langle V \rangle$ within the MCL, maximum total magnetic field strength B_{max} and average magnetic field $\langle B \rangle$ within the MCL. Brackets for t_{FW1} giving t_{MCL} values at OMNI and STEREO-B indicate that, if present, the pressure wave "FW1" coincides with the leading edge of the MCL.

Spacecraft	t_{FW1}	t_{MCL}	t_{CIR}	t_{RW}	$\langle V \rangle$	B_{max}	$\langle B \rangle$
STEREO-A	3 Jul 07:40	3 Jul 16:16	4 Jul 07:00	4 Jul 22:00	350	13	7
OMNI	(3 Jul 11:00)	3 Jul 11:00	3 Jul 19:00	4 Jul 08:10	346	11	9
STEREO-B	(3 Jul 04:00)	3 Jul 04:00	3 Jul 14:10	4 Jul 08:00	360	10	7

Table 3. Magnetic sector and electron pitch angle characteristics for each part of the transient and flux-rope orientations for the MCL at each spacecraft.

	Magnetic sector and electron pitch angle characteristics			Flux-rope orientation
	Before	MCL	After	
STEREO-A	Away, 0°	Towards, 180°	Towards 180°	North–west–south (NWS)
ACE (OMNI)	Away, 0°	Towards, 180°	Towards, 180°	North–west–south (NWS)
STEREO-B	Away, 0° with brief reversals, 0–180°	Towards, 180° (with spreading)	Towards, 180° (with spreading)	North–west–south (NWS)

terpretation of the magnetic topology of the field lines local to the spacecraft. The flux-rope orientation and characteristics are listed in Table 3.

At STEREO-A, the local orientation of the MCL normalised magnetic field vector, as shown in panels (c) and (d) of Fig. 3, turns from north ($\boldsymbol{B_N} > 0$) to west ($\boldsymbol{B_T} > 0$) to south ($\boldsymbol{B_N} < 0$) on the cloud's axis. This flux-rope cloud can be interpreted as a north–west–south (NWS) cloud with left-handed (negative) helicity. In panel (c) the (normalised) $\boldsymbol{B_R}$ component of the magnetic field is mostly negative during and after the MCL. In panel (j) we find the streaming of electrons at a pitch angle of 180° during the MCL and CIR and behind those structures, which confirms that STEREO-A is in the towards sector, north of the HCS, at this point. The lack of counter-streaming in the MCL suggests that the magnetic field lines are open; thus only one end of the magnetic field lines which form the flux rope is rooted at the Sun. A magnetic field reversal with electrons reversing in pitch angle from 0 to 180° appears close to the start of the MCL. Thus, the reversal is likely to be a crossing of the HCS (see Crooker et al., 1993). This can indicate that the MCL is acting as an occlusion in the current sheet.

At OMNI, the normalised magnetic field, shown in panels (c, d) of Fig. 2, turns from north ($\boldsymbol{B_Z} > 0$) to west ($-\boldsymbol{B_Y} > 0$) to south ($\boldsymbol{B_Z} < 0$) in the MCL, again indicating a NWS cloud with left-handed (negative) helicity. The ACE electron pitch angle data and magnetic field vector data in panels (g) and (b)–(d) of Fig. 5, respectively, show a similar result to STEREO-A, with outward magnetic field and streaming at 0° before the MIR event (away sector) and inward field and streaming at 180° during and after the event (towards sector), indicating that ACE had crossed the HCS close to the start of the MCL and is likely north of the HCS when the MCL is observed.

Similarly, at STEREO-B, in panels (c) and (d) of Fig. 4, we observe the normalised magnetic field turn from north ($\boldsymbol{B_N} > 0$) to west ($\boldsymbol{B_T} > 0$) to south ($\boldsymbol{B_N} < 0$), indicating a NWS cloud and a bipolar flux rope with a low inclination and left-handed (negative) helicity. The (normalised) $\boldsymbol{B_R}$ component of the magnetic field (panel b) is mostly negative during and after the MCL, again indicating that the magnetic field within the MCL is predominantly orientated towards the Sun. We observe electrons streaming unidirectionally at a pitch angle of 180° along field lines (panel j), albeit with some spreading, indicating a location predominantly in the towards sector of the Sun, north of the sector boundary. While again the HCS crossing appears to coincide with the start of the MCL, ahead of the MCL there are magnetic field sign changes associated with brief pitch angle reversals, indicating more structure in the field and electron data than at the other spacecraft. A main field reversal, seen first in $\boldsymbol{B_R}$ turning negative, is observed around 18:30 UT on 2 July, about 9.5 h ahead of the MCL, with electrons streaming at 180°. From 21:00 UT, the magnetic field turns back and forth, while the electrons are counter-streaming. From 3 July, another main reversal is observed, with $\boldsymbol{B_R}$ turning back to positive and with electrons streaming at 0°. Those field reversals suggest multiple folds in the magnetic field.

3 Analysis of combined MCL–CIR structures: MIRs

In this section, we address the presence of the CIR, observed at all three near-ecliptic spacecraft, in more detail and focus

on how this combines with the transient presented earlier to become an MIR.

3.1 Interaction regions

In the near-ecliptic spacecraft observations, it is clear that, in addition to the presence of a MCL, the in situ observations resemble a CIR (Pizzo and Gosling, 1994). Despite the lack of CIR forward waves at STEREO-B and OMNI, we are able to match distinct magnetic field rotations and pressure waves across the observations. There is one missing property, however. CIRs traditionally show high plasma beta (Borovsky and Denton, 2006). Here we observe a low plasma beta, which is a distinct signature of ICMEs and MC(L)s.

One piece of evidence to indicate the presence and influence of a CIR is given by the arrival timings. This evidence is provided by the observation that the MCL arrives at STEREO-B first and then Earth and STEREO-A, even though STEREO-B is the furthest of the near-Earth spacecraft from the Sun. We expect, and in this case observed, timings consistent with a CIR in the solar wind for a MCL that is greatly influenced by its surrounding solar wind. In cases where CMEs are compressed by HSSs, we can reasonably expect that the magnetic field lines joining the leading edge of the CME to the Sun are forced to co-rotate due to the high pressures induced by the compressive effects of the HSS.

These complex interactions offer a probable explanation as to why the event is relatively short, with little compression ahead of the MCL (an ICME front sheath region can only be found at STEREO-A) and why it is also difficult to disentangle the structure in the in situ data without comparison across different spacecraft. The transients are not reported by any in situ ICME catalogues relating to the near-ecliptic spacecraft as it is unlikely to have been spotted by usual automated methods, and the event duration may be too short to meet catalogue criteria. Kilpua et al. (2012) found that ICME-like transients (in contrast to ICMEs) occur more closely to CIRs.

3.2 Length scale and expansion speed

Analysis of the MIR signatures near the ecliptic plane shows that they have two to three distinct regions: (1) a front sheath FS (at STEREO-A only), (2) a MCL, and (3) a subsequent compression region created by the interaction between the MCL and a HSS. In order to compare these, we calculate the length scale of each region for each set of observations by taking the mean velocity of the region multiplied by the duration of the region, with the standard deviation included for reference. Durations can be obtained from Table 2, and the estimated length scales for each of the regions at each spacecraft are presented in Table 4.

The MCL extents are relatively short across all observations, ranging between 0.07–0.12 AU; the compression is due to the CIR. This is much smaller than the 0.2–0.3 AU MC average at 1 AU (Lepping et al., 1990; Owens et al., 2005).

Additionally, for the MIR or ICME-CIR as a whole, we estimate the length scale of the disturbance to be 0.23–0.37 AU. There is significantly more disturbance and a larger front sheath (FS) region at STEREO-A (there is no front sheath at OMNI and STEREO-B).

Finally, the mean expansion speed, V_{exp}, calculated as half of the difference between the speed of the leading and trailing edge of the MCL, is negative for all spacecraft, indicative of compression (see Table 4). The measure of compression is increasing from west to east ($V_{\mathrm{exp}} = [-7, -22.3, -76.5]\,\mathrm{km\,s^{-1}}$). Such compression is common in transients entrained in CIRs.

4 Multi-spacecraft analysis of dynamics and evolution

4.1 Modelling and predictions from remote-sensing observations

To investigate connections to the Sun, Fig. 6 displays various Carrington maps at the time of the event (Rotation 2058). Panels (c)–(e) show maps derived from the photospheric magnetic field (panel a) using a potential field source surface (PFSS) model with a spherical source surface at 2.5 $R_{\odot}$. For ease of comparison, panel (b) presents a map of coronal emission, identifying bright active regions and dark coronal holes. The subsequent maps represent simulated coronal holes (panel c), the global magnetic field configuration of the corona (panel d) and the associated radial flow at 5 $R_{\odot}$ (panel e). These maps are from the "MHDweb" project of the Predictive Science Modeling Support for SECCHI and IMPACT (PREDSCI) (http://www.predsci.com, last access: 18 July 2024) (maps a and d use the photospheric field from the Global Oscillations Network Group (GONG), and maps c and e use the photospheric field from Mount Wilson Observatory).

During this period near solar minimum, the towards sector (sunward interplanetary magnetic field, IMF) is connected to the northern solar magnetic hemisphere, while the away sector (anti-sunward interplanetary magnetic field) is connected to the southern hemisphere. Assuming that it travelled to 1 AU with the HSS speed of about $600\,\mathrm{km\,s^{-1}}$, the relevant coronal hole plasma parcel for the in situ observations will be seen at the Sun 2.9 d earlier on 1 July 2007 (dashed vertical line in Fig. 6). However, it is important to note that since the MCL is observed to be moving at a lower speed of approximately $350\,\mathrm{km\,s^{-1}}$ near 1 AU, the initial launch speed of the MCL may have been even lower, possibly around 190–$300\,\mathrm{km\,s^{-1}}$, if we consider the likelihood of acceleration by the HSS after its launch, and with some uncertainty on the timing of the interaction. Taking an average transit speed of $300\,\mathrm{km\,s^{-1}}$, for instance, the MCL is mapped back to 5.8 d earlier, on 28 June 2007. On the launch date, the source re-

Table 4. Length scales given with standard deviation for the FS, MCL and CIR; their total; and the expansion velocity V_{exp} at each of the near-ecliptic spacecraft.

Spacecraft	FS			MCL			CIR			Total			V_{exp}
	(10^6 km)		(≈ AU)	(10^6 km)		(≈ AU)	(10^6 km)		(≈ AU)	(10^6 km)		(≈ AU)	(km s^{-1})
STEREO-A	10.8	±0.8	0.07	17.9	±0.36	0.12	26.8	±4.0	0.18	55.5	±12.3	0.37	−7
OMNI				10.3	±0.41	0.07	23.8	±3.2	0.16	34.3	±6.7	0.23	−22.25
STEREO-B				15.1	±1.20	0.10	36.1	±2.4	0.24	51.2	±0.8	0.34	−76.5

gion of the MCL is located across the field inversion neutral line, thus at the base of the helmet streamer belt (panels d, e). Coronal holes with inward and outward IMF polarity are on either side of the heliospheric current sheet. Solar wind ballistic mapping using OMNI shows that the HSS is associated with an equatorial coronal hole from the northern sector (panel c). For context, using an estimate for the MCL launch speed of 250 km s^{-1} and the observed HSS speed of 600 km s^{-1}, we calculate that the interaction likely began approximately at a radial distance of 0.7 AU, or about 5 d after the MCL launch.

Since the possible source regions of the MCL and HSS are centred on the disc and the STEREO spacecraft separation is relatively small, we cannot have a side view of their evolution in any coronagraphs operating at the time. However, we can still learn about the likely behaviour of disturbances (blobs entrained in a CIR) from the contemporaneous observations of adjacent heliospheric longitudes. As seen in Fig. 7, the time–elongation maps, or *J-maps*, from STEREO/SECCHI-HI-A extending from 19 June to 5 July 2007 show a nest of converging tracks, which can be interpreted as a pattern of CIR-entrained blobs. We believe the likely behaviour of the MCL structure resembles that of one of those disturbances. One cannot be more specific, but for reference, we can take one of the CIR disturbances, HSIR_STA_20070623_100341, reported in the HELCATS STEREO SIR/CIR catalogue (Plotnikov et al., 2016) (https://www.helcats-fp7.eu/catalogues/wp5_cat.html, last access: 19 October 2024). The nest of tracks overplotted in Fig. 7 corresponds to a set of blobs all travelling at the same speed as the HELCATS CIR disturbance, which is found to have a speed of 302±21 km s^{-1} (see Rouillard et al., 2010a, for more details on the uncertainty value). The timings are derived relative to that CIR with the knowledge that one of the blobs therein was fitted to be travelling at 64 ± 6° angular separation from the Sun–spacecraft line. The CIR is predicted to arrive at STEREO-B at 15:15 UT on 3 July and at STEREO-A at 03:13 UT on 4 July 2007. This is similar to the observed earlier arrival time for STEREO-B and separation of ∼ 12 h.

Another characteristic signature of the MIR, related to the MCL nature, is the identification of the sector boundaries in the magnetic field and the near-ecliptic electron pitch angle data (Figs. 3–5). The data show that the magnetic field is anti-sunward before and sunward during and after the MCL and CIR, which is consistent with the crossing of the HCS near the start of the MCL. Sector boundaries are often found just upstream of CIRs or having just been swept up by the forward waves of CIRs since they are embedded in the slow wind into which the fast wind is running to create the CIR (Pizzo and Gosling, 1994). The proximity of the sector boundary crossing to the start of the MCL is also consistent with a flux rope, originating from the streamer belt below the sector boundary as a result of reconnection, locally replacing the HCS, while expanding outwards (Crooker and Intriligator, 1996; Crooker et al., 1998, 2004; Foullon et al., 2011). It is thus likely that this MIR is the result of the MCL interacting with both the CIR and the HCS near the ecliptic plane.

4.2 Comparative observations across spacecraft

The in situ measurements are consistent, with one or more structures developing between spacecraft, suggesting that MCL signatures may not correspond to the same structure. About two to six streamer blobs per day are recorded during solar minimum and maximum conditions, respectively (e.g. Rouillard et al., 2010a, at solar minimum). In this period of solar minimum, there could be two blobs released with a 12 h offset between them, from the base of the same streamer. The 12 h difference observed between the arrival of the MCLs at STEREO-B and STEREO-A could potentially support a scenario where, for instance, STEREO-B or OMNI (Earth) and STEREO-A encounter different blobs from the same streamer. The transient observed at STEREO-A is then the younger and most likely equivalent perturbation to the one observed at STEREO-B in a family of blobs.

However it is also more likely that we are presented with the same blob. Figure 7 shows a few significant families of tracks (each family being associated with the passage of a single CIR). Tracks that propagate beyond 60° of elongation indicate transients entrained by a HSS. Taking the family of tracks highlighted as an example, it is not clear that one can observe a set of density perturbations with a 12 h interval beyond 60° of elongation, but this could be due to instrument sensitivity.

Moreover, STEREO-A, OMNI (Earth) and STEREO-B are separated by 0.11 AU radially and less than 16.6° in longitude (less than 0.32 AU in the east–west direction). The

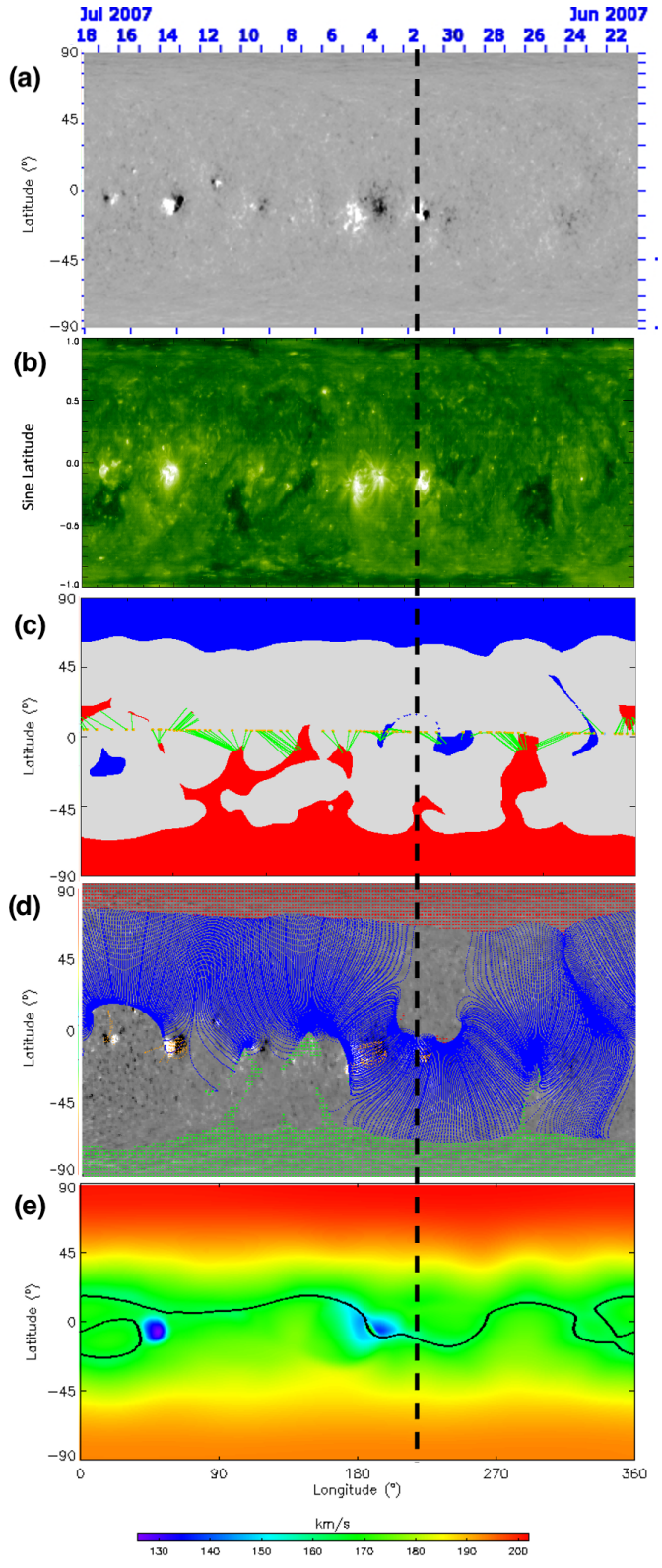

Figure 6. Carrington (synoptic) maps for Rotation 2058 showing **(a)** the photospheric magnetic field from GONG, **(b)** 195 Å EUV emission from SoHO/EIT (Hess Webber et al., 2014), **(c)** coronal hole polarities (blue negative, red positive) with Earth mapped back to the Sun (solar wind ballistic mapping in green using OMNI), **(d)** the PFSS model-derived global magnetic field configuration and **(e)** radial flow at 5 $R_\odot$ together with the projected neutral line on the source surface from PREDSCI/MHDweb. The dashed vertical line indicates the approximate Carrington longitude and time corresponding to the source of the HSS in the corona at 600 km s^{-1}.

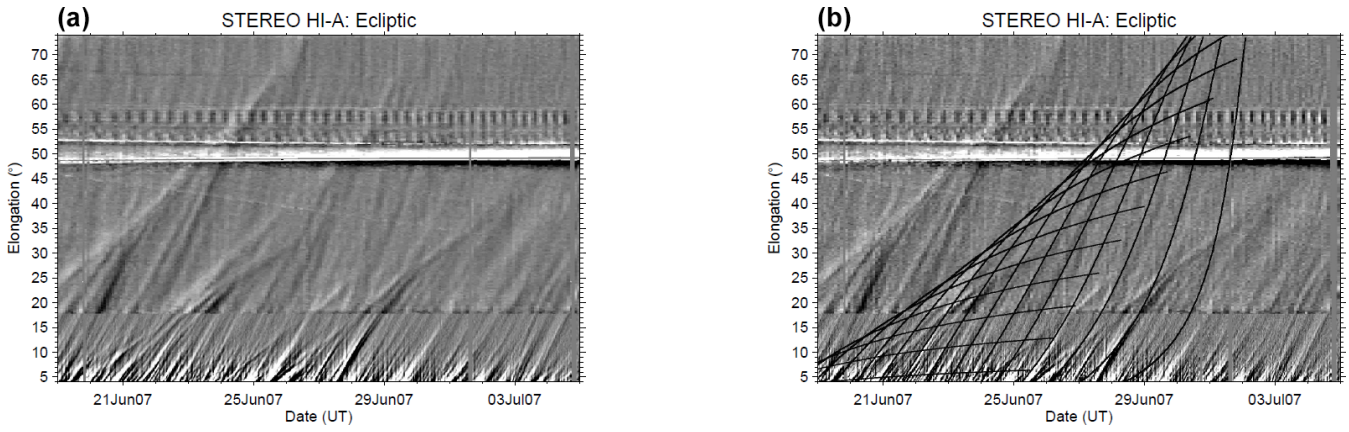

Figure 7. STEREO/SECCHI/HI-A J-maps for the period from 19 June to 5 July 2007 constructed in the ecliptic plane at a PA of 280°: **(a)** without and **(b)** with tracks superimposed. The tracks correspond to a set of blobs all travelling at the same speed as the blob that corresponds to HELCATS CIR HSIR_STA_20070623_100341, which travels at 64° angular separation from the Sun–spacecraft line. The trajectories are derived from 180 to 0° separation angles from the Sun–spacecraft line, in steps of 10°. Each blob is tracked over a somewhat arbitrary time of 10 d.

magnetic orientation analysis (Sect. 2.3) indicates that, for each spacecraft observation, the MCL's cloud axis is in the ecliptic plane, and its major size extends in the longitudinal direction, while its cross-section is compressed along the HCS. The distance the MCL travels in 12 h at the radial speed of 350 km s^{-1} is 0.10 AU. Assuming that the leading edge of the MCL reaches STEREO-B just as its trailing edge passes STEREO-A gives a minimum major size estimate of 0.33 AU. The actual structure could be larger. According to the findings of Liu et al. (2006), the cross-section aspect ratio of MCs is estimated to be no smaller than 6 : 1. Applied to our case, MCL transverse extents for all three observations are estimated to range between 0.42–0.72 AU at the minimum, which is larger than the minimum major size estimate.

Thus our event allows the comparison of MIR observations at different radial distances due to the small longitudinal separation relative to the scale size of the MCL. This comparison effectively maps the interactions of structures across a radial distance of 0.11 AU. The in situ measurements are not to be interpreted as observing the exact same structure crossing all three spacecraft at different longitudes for the same radial distance, but they are consistent with different cross-sections of the same structure or of potentially two equivalent structures evolving from the same family, crossing all three spacecraft. This allows us to infer the evolution of such structure radially. In Fig. 8, the MIR is shown as the result of the MCL interacting with both the CIR and the HCS. Moving from west to east (right to left), observations from different locations provide snapshots of the interaction between the CIR and MCL. As we move downstream from STEREO-A to OMNI (Earth) to STEREO-B, we can see the extent of this interaction.

At the earlier stage of interaction, specifically at STEREO-A, a forward wave and front sheath are produced ahead of the MCL, and a reverse wave is found at the back of the CIR as a result of the interaction with the HSS.

In the next stages, at Earth and STEREO-B, the MCLs are smaller and more turbulent, and the main sector boundary crossing appears to coincide with the start of the MCL (without a sheath).

Finally, in the later stage at STEREO-B, the MCL appears to be fully entrained in the CIR. Notably, the higher speed of the MCL at STEREO-B compared to the other spacecraft is observed. Ahead of the MCL, small-scale structures in the field and electron data are indicative of multiple magnetic folds, possibly resulting from greater interactions with the HCS (e.g. produced by interchange reconnection with the HCS).

Therefore, the MIR variations between spacecraft demonstrate the radial evolution of the MIR, with the HSS increasingly catching up with the MCL from STEREO-A to Earth and STEREO-B.

5 Conclusions

Using remote-sensing and in situ observations and across multiple near-ecliptic spacecraft, along with complementary analysis methods, we have investigated a MCL observed in situ on 3–4 July 2007 near the ecliptic plane. The MCL was found to be entrained in a CIR from the northern towards sector, which created a MIR. The MCL showed negative mean expansion speeds, indicative of compression increasing from west to east (-7, -22.3, -76.5 km s^{-1}).

This type of small-scale MCL–CIR system is not uncommon, and the prevalence of small flux ropes caught within the leading edge of CIRs observed in situ is discussed by Rouillard et al. (2009). They confirmed that the HI observes CIRs in difference images via small-scale transients caught

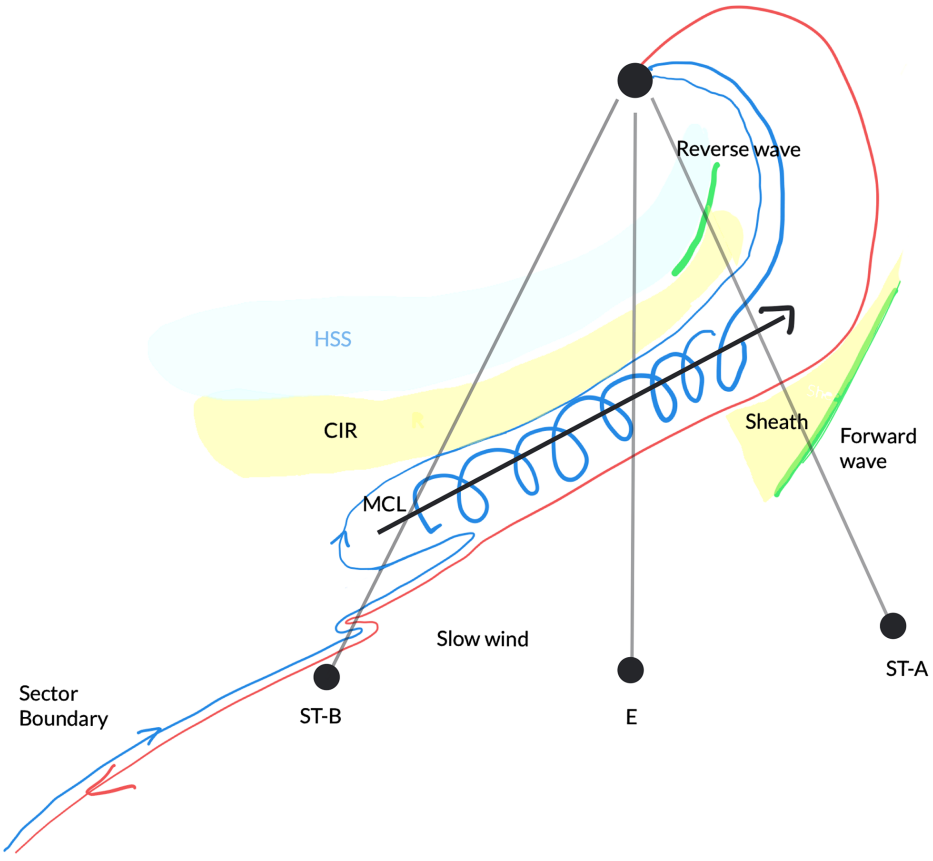

Figure 8. Sketch of the MIRs observed at different longitudes near the ecliptic plane, at STEREO-B, Earth and STEREO-A. The view is from the solar north pole. The MIR is shown as the result of the MCL interacting with both the CIR and the HCS. The MCL flux rope with the main axis (black arrow) pointing westward is embedded between the towards northern sector (blue) and away southern sector (red) field lines. The MIR variations across the spacecraft demonstrate the progression of the interaction between the CIR and MCL from west to east.

up in the compression region. In fact, Rouillard et al. (2009) reported on a small-scale transient entrained by a CIR that has parallels with our event. Their event was observed later on 20 July 2007. Resemblances between the two events include similar flux-rope profiles observed at STEREO-A, with a clear reversal of the polarity of magnetic field lines and a change of suprathermal electron pitch angle from 0 to 180° at the start of the MCL. For the event presented by Rouillard et al. (2009), there is no corresponding MC or MCL at the other spacecraft during the same CIR passage, except for a peak in the magnetic field ahead of the CIR, which may be related to a shock driven by the interaction.

In our case, the MCL–CIR system appears more complex and extended, qualifying as a small-scale MIR, based on the criteria of Burlaga et al. (2003) for MIR terminology at 1 AU. We observed clear MCLs at STEREO-B and OMNI, which were smaller and more turbulent than at STEREO-A. At all spacecraft, the local orientations of the MCL magnetic field vector turned from north to west to south on the cloud's axis, indicating a north–west–south (NWS) cloud with left-handed (negative) helicity.

By comparing data from STEREO-A, OMNI/ACE and STEREO-B with less than 16.6° separation angle in longitude (less than 0.32 AU in the east–west direction), the study mapped interactions of these structures across 0.11 AU in radial distance. This event allowed for the comparison of MIR observations at different longitudes showing differences in size, (negative) expansion speed, formation of sheath, and the presence of forward and reverse waves and small-scale structuring and providing a sequence of different interaction stages progressing radially. Thus, the study demonstrated the radial evolution of the MIR, with the HSS increasingly catching up with the MCL from STEREO-A to Earth and STEREO-B. The observed MCLs in the solar wind undergo interactions with the HSS, resulting first in shock waves and front sheath and then with increasing compressions from

the HSS, leading to increased turbulence and magnetic folds (possibly from interchange reconnection with the HCS).

This observed evolution of the MCL–CIR interaction across the three spacecraft provides a unique glimpse into the "ageing" process of these structures. The progression from a distinct MCL with a clear sheath at STEREO-A to a more turbulent, fully entrained structure at STEREO-B demonstrates how rapidly these interactions can evolve over relatively small spatial and temporal scales. Recent studies using Parker Solar Probe (PSP) and Solar Orbiter (SO) data have shown similar rapid evolution of small-scale magnetic structures in the inner heliosphere (e.g. Telloni et al., 2022; Ventura et al., 2023), though typically at closer distances to the Sun. Our observations extend this understanding to 1 AU, highlighting the dynamic nature of solar wind structures even at Earth's orbit. The observed ageing process of the MCL–CIR interaction may have implications for the geoeffectiveness of these structures. As the MCL becomes more entrained and turbulent, its magnetic field structure is likely to become less coherent. This could potentially reduce its ability to drive strong geomagnetic activity, as the most geoeffective magnetic clouds typically have strong, smoothly rotating magnetic fields (Huttunen et al., 2005). However, the increased compression and turbulence might also lead to enhanced local plasma density and temperature, which could compensate for the reduced magnetic field coherence in terms of geoeffectiveness. Further statistical studies would be needed to fully understand the relationship between this ageing process and geomagnetic impact.

The findings emphasise the complex nature of solar wind structures and their interactions, particularly the formation and evolution of MIRs at 1 AU, contributing to our understanding of the formation processes starting at the Sun. They highlight the importance of using a comprehensive multi-spacecraft approach, which is essential for distinguishing between MCs/MCLs and their solar wind environments and for identifying connections between events observed in the heliosphere. For this specific event, we have observed a simultaneous event as presented in Maunder et al. (2022), where a multi-spacecraft study of a mid-latitude CME allowed for analysis of remote-sensing observations from the twin STEREO-A and STEREO-B spacecraft, as well as its subsequent in situ counterpart outside the ecliptic plane, at Ulysses. Connecting these two events has posed challenges (Maunder, 2023).

Potential extensions, but beyond the scope of this study, could include considering energetic particle effects and interplanetary scintillation observations (e.g. Richardson, 2018, and references therein). However, the study shows that, compared to the identification of ICMEs and MIRs, the origin and formation of ICME-like transients and ICME substructures are less well understood.

Data availability. The data sets generated during and/or analysed during the current study are available from the corresponding author on reasonable request.

Author contributions. MLM was responsible for data curation, formal analysis, investigation, data visualisation and writing the original draft of the manuscript. CF supervised the research project, contributed to its conceptualisation, assisted with visualisation, and provided substantial writing contributions along with critical review and editing of the manuscript. RF, DB and JAD contributed to the investigation, data visualisation, and review and editing of the manuscript.

Competing interests. The contact author has declared that none of the authors has any competing interests.

Disclaimer. Publisher's note: Copernicus Publications remains neutral with regard to jurisdictional claims made in the text, published maps, institutional affiliations, or any other geographical representation in this paper. While Copernicus Publications makes every effort to include appropriate place names, the final responsibility lies with the authors.

Acknowledgements. The HI instruments on STEREO were developed by a consortium that comprised the Rutherford Appleton Laboratory (UK), the University of Birmingham (UK), Centre Spatial de Liège (CSL, Belgium) and the Naval Research Laboratory (NRL, USA). The STEREO/SECCHI project, of which HI is a part, is an international consortium led by NRL. We recognise the support of the UK Space Agency for funding STEREO/HI post-launch support activities in the UK. This study includes data acquired by GONG instruments operated by NISP, NSO, AURA and NSF, with contribution from NOAA. It also includes data from the synoptic programme at the 150-foot solar tower of the Mt. Wilson Observatory. The Mt. Wilson 150-foot solar tower is operated by UCLA, with funding from NASA, ONR and NSF, under agreement with the Mt. Wilson Institute.

Data analysis was performed with the AMDA science analysis system provided by the Centre de Données de la Physique des Plasmas (CDPP) supported by CNRS; CNES; Observatoire de Paris; and Université Paul Sabatier, Toulouse.

Financial support. This research has been supported by the Science and Technology Facilities Council (grant no. 2072927).

Review statement. This paper was edited by Ioannis A. Daglis and reviewed by Angelos Vourlidas and one anonymous referee.

References

Borovsky, J. E. and Denton, M. H.: Differences between CME-driven storms and CIR-driven storms, J. Geophys. Res.-Space, 111, A07S08, https://doi.org/10.1029/2005JA011447, 2006.

Bothmer, V. and Schwenn, R.: The structure and origin of magnetic clouds in the solar wind, Ann. Geophys., 16, 1–24, https://doi.org/10.1007/s00585-997-0001-x, 1998.

Burlaga, L., Berdichevsky, D., Gopalswamy, N., Lepping, R., and Zurbuchen, T.: Merged interaction regions at 1 AU, J. Geophys. Res.-Space, 108, 1425, https://doi.org/10.1029/2003JA010088, 2003.

Burlaga, L. F.: Magnetohydrodynamic Processes in the Outer Heliosphere, Space Sci. Rev., 39, 255–316, https://doi.org/10.1007/BF00173902, 1984.

Burlaga, L. F.: Merged Interaction Regions, in: Interplanetary Magnetohydrodynamics, Oxford University Press, ISBN 9780195084726, https://doi.org/10.1093/oso/9780195084726.003.0008, 1995.

Burlaga, L. F.: Terminology for ejecta in the solar wind, EOS Transactions, 82, 433–435, https://doi.org/10.1029/01EO00265, 2001.

Crooker, N. U. and Intriligator, D. S.: A magnetic cloud as a distended flux rope occlusion in the heliospheric current sheet, J. Geophys. Res., 101, 24343–24348, https://doi.org/10.1029/96JA02129, 1996.

Crooker, N. U., Siscoe, G. L., Shodhan, S., Webb, D. F., Gosling, J. T., and Smith, E. J.: Multiple heliospheric current sheets and coronal streamer belt dynamics, J. Geophys. Res., 98, 9371–9382, https://doi.org/10.1029/93JA00636, 1993.

Crooker, N. U., Gosling, J. T., and Kahler, S. W.: Magnetic clouds at sector boundaries, J. Geophys. Res., 103, 301–306, https://doi.org/10.1029/97JA02774, 1998.

Crooker, N. U., Kahler, S. W., Larson, D. E., and Lin, R. P.: Large-scale magnetic field inversions at sector boundaries, J. Geophys. Res.-Space, 109, A03108, https://doi.org/10.1029/2003JA010278, 2004.

Dasso, S., Mandrini, C. H., Démoulin, P., and Luoni, M. L.: A new model-independent method to compute magnetic helicity in magnetic clouds, Astron. Astrophys., 455, 349–359, https://doi.org/10.1051/0004-6361:20064806, 2006.

Davies, E. E., Forsyth, R. J., Good, S. W., and Kilpua, E. K. J.: On the Radial and Longitudinal Variation of a Magnetic Cloud: ACE, Wind, ARTEMIS and Juno Observations, Sol. Phys., 295, 157, https://doi.org/10.1007/s11207-020-01714-z, 2020.

DiBraccio, G. A., Slavin, J. A., Imber, S. M., Gershman, D. J., Raines, J. M., Jackman, C. M., Boardsen, S. A., Anderson, B. J., Korth, H., Zurbuchen, T. H., McNutt, R. L., and Solomon, S. C.: MESSENGER observations of flux ropes in Mercury's magnetotail, Plan. Space Sci., 115, 77–89, https://doi.org/10.1016/j.pss.2014.12.016, 2015.

Eyles, C. J., Harrison, R. A., Davis, C. J., Waltham, N. R., Shaughnessy, B. M., Mapson-Menard, H. C. A., Bewsher, D., Crothers, S. R., Davies, J. A., Simnett, G. M., Howard, R. A., Moses, J. D., Newmark, J. S., Socker, D. G., Halain, J.-P., Defise, J.-M., Mazy, E., and Rochus, P.: The Heliospheric Imagers Onboard the STEREO Mission, Sol. Phys., 254, 387–445, https://doi.org/10.1007/s11207-008-9299-0, 2009.

Farrugia, C. J., Berdichevsky, D. B., Möstl, C., Galvin, A. B., Leitner, M., Popecki, M. A., Simunac, K. D. C., Opitz, A., Lavraud, B., Ogilvie, K. W., Veronig, A. M., Temmer, M., Luhmann, J. G., and Sauvaud, J. A.: Multiple, distant (40°) in situ observations of a magnetic cloud and a corotating interaction region complex, J. Atmos. Sol.-Terr. Phys., 73, 1254–1269, https://doi.org/10.1016/j.jastp.2010.09.011, 2011.

Feng, H. Q., Wu, D. J., and Chao, J. K.: Size and energy distributions of interplanetary magnetic flux ropes, J. Geophys. Res.-Space, 112, A02102, https://doi.org/10.1029/2006JA011962, 2007.

Foullon, C., Owen, C. J., Dasso, S., Green, L. M., Dandouras, I., Elliott, H. A., Fazakerley, A. N., Bogdanova, Y. V., and Crooker, N. U.: Multi-Spacecraft Study of the 21 January 2005 ICME. Evidence of Current Sheet Substructure Near the Periphery of a Strongly Expanding, Fast Magnetic Cloud, Sol. Phys., 244, 139–165, https://doi.org/10.1007/s11207-007-0355-y, 2007.

Foullon, C., Lavraud, B., Wardle, N. C., Owen, C. J., Kucharek, H., and et al.: The Apparent Layered Structure of the Heliospheric Current Sheet: Multi-Spacecraft Observations, Sol. Phys., 259, 389–416, https://doi.org/10.1007/s11207-009-9452-4, 2009.

Foullon, C., Lavraud, B., Luhmann, J. G., Farrugia, C. J., Retinò, A., Simunac, K. D. C., Wardle, N. C., Galvin, A. B., Kucharek, H., Owen, C. J., Popecki, M., Opitz, A., and Sauvaud, J.-A.: Plasmoid Releases in the Heliospheric Current Sheet and Associated Coronal Hole Boundary Layer Evolution, Astrophys. J., 737, 16 pp., https://doi.org/10.1088/0004-637X/737/1/16, 2011.

Galvin, A. B., Kistler, L. M., Popecki, M. A., Farrugia, C. J., Simunac, K. D. C., Ellis, L., Möbius, E., Lee, M. A., Boehm, M., Carroll, J., Crawshaw, A., Conti, M., Demaine, P., Ellis, S., Gaidos, J. A., Googins, J., Granoff, M., Gustafson, A., Heirtzler, D., King, B., Knauss, U., Levasseur, J., Longworth, S., Singer, K., Turco, S., Vachon, P., Vosbury, M., Widholm, M., Blush, L. M., Karrer, R., Bochsler, P., Daoudi, H., Etter, A., Fischer, J., Jost, J., Opitz, A., Sigrist, M., Wurz, P., Klecker, B., Ertl, M., Seidenschwang, E., Wimmer-Schweingruber, R. F., Koeten, M., Thompson, B., and Steinfeld, D.: The Plasma and Suprathermal Ion Composition (PLASTIC) Investigation on the STEREO Observatories, Space Sci. Rev., 136, 437–486, https://doi.org/10.1007/s11214-007-9296-x, 2008.

Gazis, P. R.: Solar cycle variation in the heliosphere, Rev. Geophys., 34, 379–402, https://doi.org/10.1029/96RG00892, 1996.

Gieseler, J., Dresing, N., Palmroos, C., Freiherr von Forstner, J. L., Price, D. J., Vainio, R., Kouloumvakos, A., Rodríguez-García, L., Trotta, D., Génot, V., Masson, A., Roth, M., and Veronig, A.: Solar-MACH: An open-source tool to analyze solar magnetic connection configurations, Front. Astron. Space Sci., 9, 1058810, https://doi.org/10.3389/fspas.2022.1058810, 2023.

Gosling, J. T.: Coronal mass ejections in the solar wind at high solar latitudes: an overview, in: Solar Dynamic Phenomena and Solar Wind Consequences, Proceedings of the Third SOHO Workshop, Estes Park, Colorado, USA, 26-29 September 1994, 275, ESA Special Publication, Vol. 373, ISBN:9290921757, 1994.

Gosling, J. T., Hildner, E., MacQueen, R. M., Munro, R. H., Poland, A. I., and Ross, C. L.: Direct Observations of a Flare Related Coronal and Solar Wind Disturbance, Sol. Phys., 40, 439–448, https://doi.org/10.1007/BF00162390, 1975.

Gosling, J. T., Bame, S. J., McComas, D. J., Phillips, J. L., Scime, E. E., Pizzo, V. J., Goldstein, B. E., and Balogh, A.: A forward-reverse shock pair in the solar wind driven by over-expansion of a coronal mass ejection: Ulysses observations, Geophys. Res. Lett., 21, 237–240, https://doi.org/10.1029/94GL00001, 1994.

Hess Webber, S. A., Karna, N., Pesnell, W. D., and Kirk, M. S.: Areas of Polar Coronal Holes from 1996 Through 2010, Sol. Phys., 289, 4047–4067, https://doi.org/10.1007/s11207-014-0564-0, 2014.

Howard, T.: Coronal Mass Ejections: An Introduction, Springer New York, NY, https://doi.org/10.1007/978-1-4419-8789-1, 2011.

Huttunen, K. E. J., Schwenn, R., Bothmer, V., and Koskinen, H. E. J.: Properties and geoeffectiveness of magnetic clouds in the rising, maximum and early declining phases of solar cycle 23, Ann. Geophys., 23, 625–641, https://doi.org/10.5194/angeo-23-625-2005, 2005.

Kaiser, M. L., Kucera, T. A., Davila, J. M., St. Cyr, O. C., Guhathakurta, M., and Christian, E.: The STEREO Mission: An Introduction, Space Sci. Rev., 136, 5–16, https://doi.org/10.1007/s11214-007-9277-0, 2008.

Kay, C., Nieves-Chinchilla, T., Hofmeister, S. J., Palmerio, E., and Ledvina, V. E.: A Series of Advances in Analytic Interplanetary CME Modeling, Space Weather, 21, e2023SW003647, https://doi.org/10.1029/2023SW003647, 2023.

Kilpua, E., Koskinen, H. E. J., and Pulkkinen, T. I.: Coronal mass ejections and their sheath regions in interplanetary space, Living Rev. Sol. Phys., 14, 83 pp., https://doi.org/10.1007/s41116-017-0009-6, 2017.

Kilpua, E. K. J., Jian, L. K., Li, Y., Luhmann, J. G., and Russell, C. T.: Observations of ICMEs and ICME-like Solar Wind Structures from 2007–2010 Using Near-Earth and STEREO Observations, Sol. Phys., 281, 391–409, https://doi.org/10.1007/s11207-012-9957-0, 2012.

King, J. H. and Papitashvili, N. E.: Solar wind spatial scales in and comparisons of hourly Wind and ACE plasma and magnetic field data, J. Geophys. Res.-Space, 110, A02104, https://doi.org/10.1029/2004JA010649, 2005.

Lavraud, B., Fargette, N., Réville, V., Szabo, A., Huang, J., Rouillard, A. P., Viall, N., Phan, T. D., Kasper, J. C., Bale, S. D., Berthomier, M., Bonnell, J. W., Case, A. W., de Wit, T. D., Eastwood, J. P., Génot, V., Goetz, K., Griton, L. S., Halekas, J. S., Harvey, P., Kieokaew, R., Klein, K. G., Korreck, K. E., Kouloumvakos, A., Larson, D. E., Lavarra, M., Livi, R., Louarn, P., MacDowall, R. J., Maksimovic, M., Malaspina, D., Nieves-Chinchilla, T., Pinto, R. F., Poirier, N., Pulupa, M., Raouafi, N. E., Stevens, M. L., Toledo-Redondo, S., and Whittlesey, P. L.: The Heliospheric Current Sheet and Plasma Sheet during Parker Solar Probe's First Orbit, Astrophys. J. Lett., 894, 8 pp., https://doi.org/10.3847/2041-8213/ab8d2d, 2020.

Lepping, R. P., Jones, J. A., and Burlaga, L. F.: Magnetic field structure of interplanetary magnetic clouds at 1 AU, J. Geophys. Res., 95, 11957–11965, https://doi.org/10.1029/JA095iA08p11957, 1990.

Lepping, R. P., Acũna, M. H., Burlaga, L. F., Farrell, W. M., Slavin, J. A., Schatten, K. H., Mariani, F., Ness, N. F., Neubauer, F. M., Whang, Y. C., Byrnes, J. B., Kennon, R. S., Panetta, P. V., Scheifele, J., and Worley, E. M.: The Wind Magnetic Field Investigation, Space Sci. Rev., 71, 207–229, https://doi.org/10.1007/BF00751330, 1995.

Lepping, R. P., Wu, C. C., and Berdichevsky, D. B.: Automatic identification of magnetic clouds and cloud-like regions at 1 AU: occurrence rate and other properties, Ann. Geophys., 23, 2687–2704, https://doi.org/10.5194/angeo-23-2687-2005, 2005.

Liu, Y., Richardson, J. D., Belcher, J. W., Wang, C., Hu, Q., and Kasper, J. C.: Constraints on the global structure of magnetic clouds: Transverse size and curvature, J. Geophys. Res.-Space, 111, A12S03, https://doi.org/10.1029/2006JA011890, 2006.

Lopez, R. E.: Solar cycle invariance in solar wind proton temperature relationships, J. Geophys. Res., 92, 11189–11194, https://doi.org/10.1029/JA092iA10p11189, 1987.

Luhmann, J. G., Curtis, D. W., Schroeder, P., McCauley, J., Lin, R. P., Larson, D. E., Bale, S. D., Sauvaud, J. A., Aoustin, C., Mewaldt, R. A., Cummings, A. C., Stone, E. C., Davis, A. J., Cook, W. R., Kecman, B., Wiedenbeck, M. E., von Rosenvinge, T., Acuna, M. H., Reichenthal, L. S., Shuman, S., Wortman, K. A., Reames, D. V., Mueller-Mellin, R., Kunow, H., Mason, G. M., Walpole, P., Korth, A., Sanderson, T. R., Russell, C. T., and Gosling, J. T.: STEREO IMPACT Investigation Goals, Measurements, and Data Products Overview, Space Sci. Rev., 136, 117–184, https://doi.org/10.1007/s11214-007-9170-x, 2008.

Marubashi, K.: Structure of the interplanetary magnetic clouds and their solar origins, Adv. Space Res., 6, 335–338, https://doi.org/10.1016/0273-1177(86)90172-9, 1986.

Marubashi, K.: Interplanetary Magnetic Flux Ropes and Solar Filaments, in: Coronal Mass Ejections, edited by: Crooker, N., Joselyn, J. A., and Feynman, J., https://doi.org/10.1029/GM099p0147, 1997.

Maunder, M. L.: Multi-Spacecraft Investigations of Solar and Interplanetary Coronal Mass Ejections in Complex Solar Wind Environments, Ph.D. thesis, University of Exeter, UK, http://hdl.handle.net/10871/133256 (last access: 1 December 2024), 2023.

Maunder, M. L., Foullon, C., Forsyth, R., Barnes, D., and Davies, J.: Multi-Spacecraft Observations of an Interplanetary Coronal Mass Ejection Interacting with Two Solar-Wind Regimes Observed by the Ulysses and Twin-STEREO Spacecraft, Sol. Phys., 297, 148, https://doi.org/10.1007/s11207-022-02077-3, 2022.

Möstl, C., Farrugia, C. J., Miklenic, C., Temmer, M., Galvin, A. B., Luhmann, J. G., Kilpua, E. K. J., Leitner, M., Nieves-Chinchilla, T., Veronig, A., and Biernat, H. K.: Multispacecraft recovery of a magnetic cloud and its origin from magnetic reconnection on the Sun, J. Geophys. Res.-Space, 114, A04102, https://doi.org/10.1029/2008JA013657, 2009.

Mulligan, T., Russell, C. T., and Luhmann, J. G.: Solar cycle evolution of the structure of magnetic clouds in the inner heliosphere, Geophys. Res. Lett., 25, 2959–2962, https://doi.org/10.1029/98GL01302, 1998.

Owens, M. J., Cargill, P. J., Pagel, C., Siscoe, G. L., and Crooker, N. U.: Characteristic magnetic field and speed properties of interplanetary coronal mass ejections and their sheath regions, J. Geophys. Res.-Space, 110, A01105, https://doi.org/10.1029/2004JA010814, 2005.

Palmerio, E., Scolini, C., Barnes, D., Magdalenić, J., West, M. J., Zhukov, A. N., Rodriguez, L., Mierla, M., Good, S. W., Morosan, D. E., Kilpua, E. K. J., Pomoell, J., and Poedts, S.: Multipoint Study of Successive Coronal Mass Ejections Driving Moderate Disturbances at 1 AU, Astrophys. J., 878, 15 pp., https://doi.org/10.3847/1538-4357/ab1850, 2019.

Parker, E. N.: Dynamics of the Interplanetary Gas and Magnetic Fields, Astrophys. J., 128, 664, https://doi.org/10.1086/146579, 1958.

Pizzo, V. J. and Gosling, J. T.: 3-D Simulation of high-latitude interaction regions: Comparison with Ulysses results, Geophys. Res. Lett., 21, 2063–2066, https://doi.org/10.1029/94GL01581, 1994.

Plotnikov, I., Rouillard, A. P., Davies, J. A., Bothmer, V., Eastwood, J. P., Gallagher, P., Harrison, R. A., Kilpua, E., Möstl, C., Perry, C. H., Rodriguez, L., Lavraud, B., Génot, V., Pinto, R. F., and Sanchez-Diaz, E.: Long-Term Tracking of Corotating Density Structures Using Heliospheric Imaging, Sol. Phys., 291, 1853–1875, https://doi.org/10.1007/s11207-016-0935-9, 2016.

Richardson, I. G.: Identification of Interplanetary Coronal Mass Ejections at Ulysses Using Multiple Solar Wind Signatures, Sol. Phys., 289, 3843–3894, https://doi.org/10.1007/s11207-014-0540-8, 2014.

Richardson, I. G.: Solar wind stream interaction regions throughout the heliosphere, Living Rev. Sol. Phys., 15, 95 pp., https://doi.org/10.1007/s41116-017-0011-z, 2018.

Richardson, I. G. and Cane, H. V.: Regions of abnormally low proton temperature in the solar wind (1965–1991) and their association with ejecta, J. Geophys. Res.-Space, 100, 23397–23412, https://doi.org/10.1029/95JA02684, 1995.

Rodkin, D., Slemzin, V., Zhukov, A. N., Goryaev, F., Shugay, Y., and Veselovsky, I.: Single ICMEs and Complex Transient Structures in the Solar Wind in 2010–2011, Sol. Phys., 293, 78, https://doi.org/10.1007/s11207-018-1295-4, 2018.

Rouillard, A. P., Davies, J. A., Forsyth, R. J., Rees, A., Davis, C. J., Harrison, R. A., Lockwood, M., Bewsher, D., Crothers, S. R., Eyles, C. J., Hapgood, M., and Perry, C. H.: First imaging of corotating interaction regions using the STEREO spacecraft, Geophys. Res. Lett., 35, L10110, https://doi.org/10.1029/2008GL033767, 2008.

Rouillard, A. P., Savani, N. P., Davies, J. A., Lavraud, B., Forsyth, R. J., Morley, S. K., Opitz, A., Sheeley, N. R., Burlaga, L. F., Sauvaud, J. A., Simunac, K. D. C., Luhmann, J. G., Galvin, A. B., Crothers, S. R., Davis, C. J., Harrison, R. A., Lockwood, M., Eyles, C. J., Bewsher, D., and Brown, D. S.: A Multispacecraft Analysis of a Small-Scale Transient Entrained by Solar Wind Streams, Sol. Phys., 256, 307–326, https://doi.org/10.1007/s11207-009-9329-6, 2009.

Rouillard, A. P., Davies, J. A., Lavraud, B., Forsyth, R. J., Savani, N. P., Bewsher, D., Brown, D. S., Sheeley, N. R., Davis, C. J., Harrison, R. A., Howard, R. A., Vourlidas, A., Lockwood, M., Crothers, S. R., and Eyles, C. J.: Intermittent release of transients in the slow solar wind: 1. Remote sensing observations, J. Geophys. Res.-Space, 115, A04103, https://doi.org/10.1029/2009JA014471, 2010a.

Rouillard, A. P., Lavraud, B., Sheeley, N. R., Davies, J. A., Burlaga, L. F., Savani, N. P., Jacquey, C., and Forsyth, R. J.: White Light and In Situ Comparison of a Forming Merged Interaction Region, Astrophys. J., 719, 1385–1392, https://doi.org/10.1088/0004-637X/719/2/1385, 2010b.

Russell, C. T. and Mulligan, T.: The true dimensions of interplanetary coronal mass ejections, Adv. Space Res., 29, 301–306, https://doi.org/10.1016/S0273-1177(01)00588-9, 2002.

Sanchez-Diaz, E., Rouillard, A. P., Davies, J. A., Lavraud, B., Pinto, R. F., and Kilpua, E.: The Temporal and Spatial Scales of Density Structures Released in the Slow Solar Wind During Solar Activity Maximum, Astrophys. J., 851, 17 pp., https://doi.org/10.3847/1538-4357/aa98e2, 2017.

Shugay, Y., Slemzin, V., Rodkin, D., Yermolaev, Y., and Veselovsky, I.: Influence of coronal mass ejections on parameters of high-speed solar wind: a case study, J. Space Weather Spac., 8, 13 pp., https://doi.org/10.1051/swsc/2018015, 2018.

Smith, E. J. and Wolfe, J. H.: Observations of interaction regions and corotating shocks between one and five AU: Pioneers 10 and 11, Geophys. Res. Lett., 3, 137–140, https://doi.org/10.1029/GL003i003p00137, 1976.

Stone, E. C., Frandsen, A. M., Mewaldt, R. A., Christian, E. R., Margolies, D., Ormes, J. F., and Snow, F.: The Advanced Composition Explorer, Space Sci. Rev., 86, 1–22, https://doi.org/10.1023/A:1005082526237, 1998.

Telloni, D., Zank, G. P., Stangalini, M., Downs, C., Liang, H., Nakanotani, M., Andretta, V., Antonucci, E., Sorriso-Valvo, L., Adhikari, L., Zhao, L., Marino, R., Susino, R., Grimani, C., Fabi, M., D'Amicis, R., Perrone, D., Bruno, R., Carbone, F., Mancuso, S., Romoli, M., Deppo, V. D., Fineschi, S., Heinzel, P., Moses, J. D., Naletto, G., Nicolini, G., Spadaro, D., Teriaca, L., Frassati, F., Jerse, G., Landini, F., Pancrazzi, M., Russano, G., Sasso, C., Biondo, R., Burtovoi, A., Capuano, G. E., Casini, C., Casti, M., Chioetto, P., De Leo, Y., Giarrusso, M., Liberatore, A., Berghmans, D., Auchère, F., Cuadrado, R. A., Chitta, L. P., Harra, L., Kraaikamp, E., Long, D. M., Mandal, S., Parenti, S., Pelouze, G., Peter, H., Rodriguez, L., Schühle, U., Schwanitz, C., Smith, P. J., Verbeeck, C., and Zhukov, A. N.: Observation of a Magnetic Switchback in the Solar Corona, Astrophys. J. Lett., 936, L25, https://doi.org/10.3847/2041-8213/ac8104, 2022.

Ventura, R., Antonucci, E., Downs, C., Romano, P., Susino, R., Spadaro, D., Telloni, D., Guglielmino, S. L., Capuano, G., Andretta, V., Landini, F., Jerse, G., Nicolini, G., Pancrazzi, M., Sasso, C., Da Deppo, V., Fineschi, S., Grimani, C., Heinzel, P., Moses, D., Naletto, G., Romoli, M., Stangalini, M., Teriaca, L., and Uslenghi, M.: Recurrent solar density transients in the slow wind observed with the Metis coronagraph, Astron. Astrophys., 675, 9 pp., https://doi.org/10.1051/0004-6361/202346623, 2023.

Wang, Y. M., Sheeley, N. R., Socker, D. G., Howard, R. A., and Rich, N. B.: The dynamical nature of coronal streamers, J. Geophys. Res., 105, 25133–25142, https://doi.org/10.1029/2000JA000149, 2000.

Winslow, R. M., Lugaz, N., Scolini, C., and Galvin, A. B.: First Simultaneous In Situ Measurements of a Coronal Mass Ejection by Parker Solar Probe and STEREO-A, Astrophys. J., 916, 10 pp., https://doi.org/10.3847/1538-4357/ac0821, 2021.

Wu, C. C., Lepping, R. P., and Gopalswamy, N.: Relationships Among Magnetic Clouds, CMES, and Geomagnetic Storms, Sol. Phys., 239, 449–460, https://doi.org/10.1007/s11207-006-0037-1, 2006.

Zurbuchen, T. H. and Richardson, I. G.: In-Situ Solar Wind and Magnetic Field Signatures of Interplanetary Coronal Mass Ejections, Space Sci. Rev., 123, 31–43, https://doi.org/10.1007/s11214-006-9010-4, 2006.